SUPPORTING MATERIAL

How an inhibitor bound to subunit interface alters triosephosphate isomerase dynamics.

Zeynep Kurkcuoglu[1], Doga Findik[1], Ebru Demet Akten[2], Pemra Doruker[1*]

[1] Department of Chemical Engineering and Polymer Research Center, Bogazici University Bebek, 34342, Istanbul, Turkey

[2] Department of Bioinformatics and Genetics, Faculty of Engineering and Natural Sciences, Kadir Has University, Cibali, Fatih, 34083 Istanbul, Turkey

*Corresponding author: Tel: +90-212-359-7002
Fax: +90-212-257-5032
E-mail address: doruker@boun.edu.tr (P. Doruker)

FIGURES

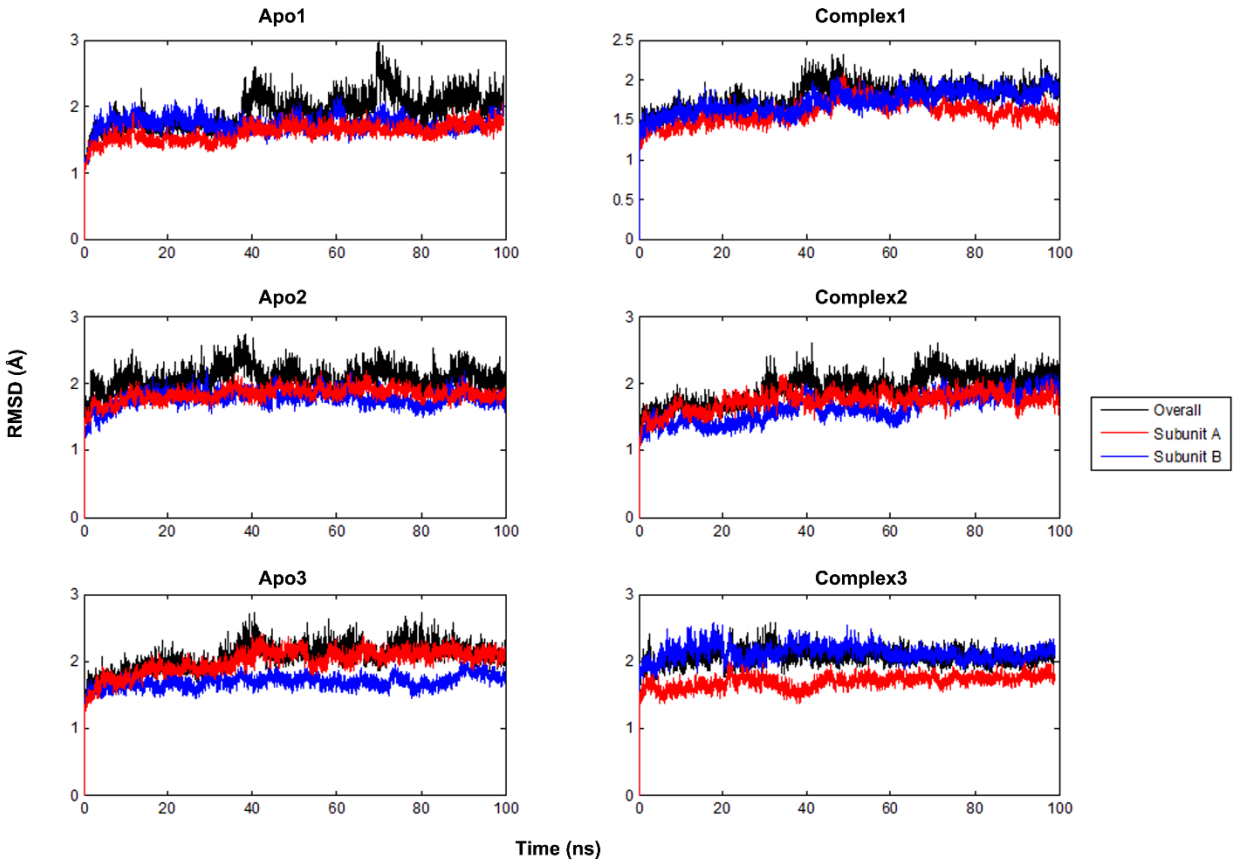

Figure S1. Heavy-atom based RMSD profiles for MD runs. RMSDs for each run are calculated after alignment of the snapshots onto its minimized initial structure based on heavy atoms. Overall alignment and RMSD profiles are shown in black. Monomer-based alignment and RMSDs are shown in red (blue) for subunit A (B). Relatively larger deviations in the dimer are indicative of inter-subunit motions.

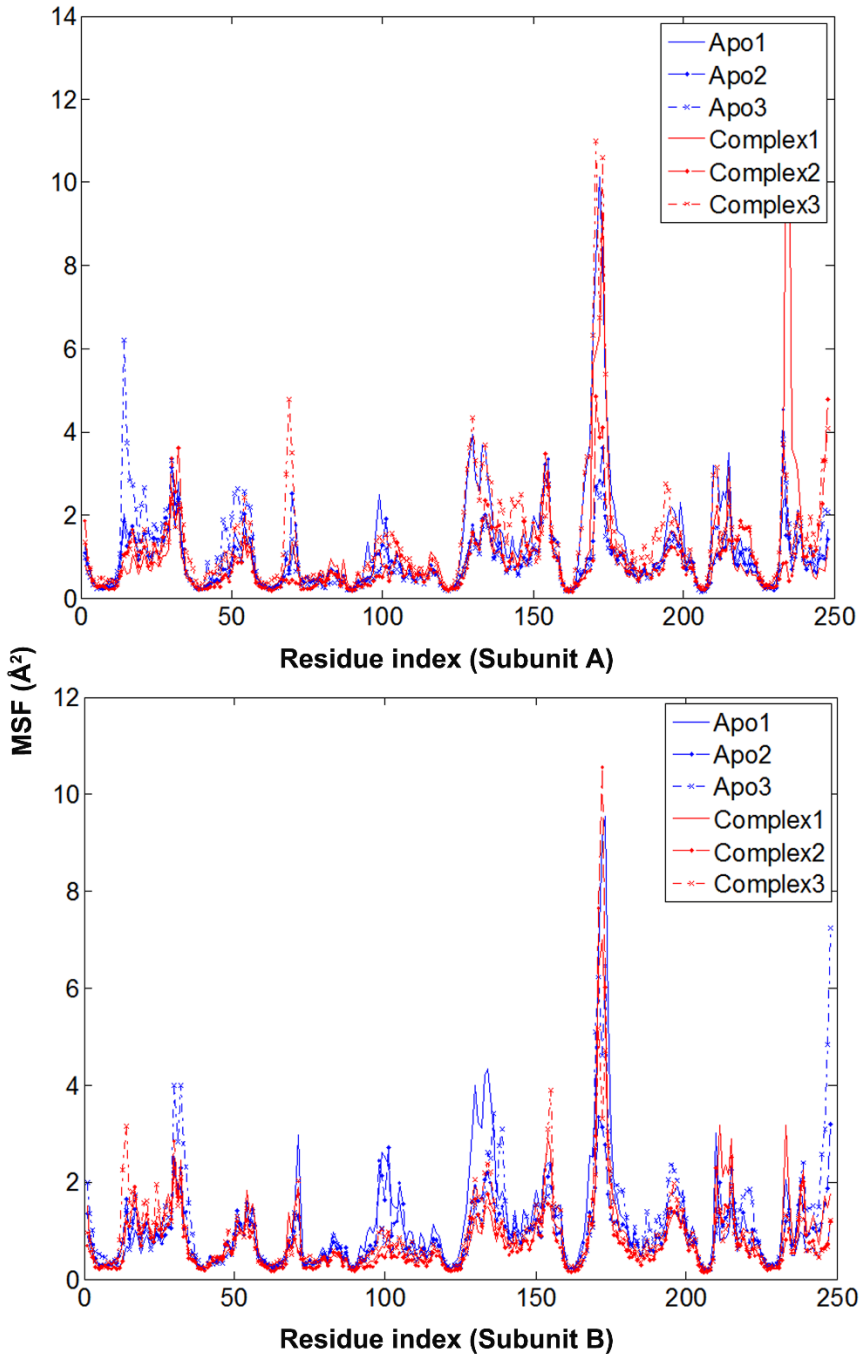

Figure S2. Mean square fluctuations (MSF) of apo and complex TIM for each run. We have performed two-way ANOVA to test the null hypothesis that presence of ligand has no effect on residue MSF. Two-way ANOVA revealed that the probability to accept the null hypothesis is 0.0185. Since p-value is less than 0.05, it is statistically significant to reject the null hypothesis, i.e. presence of ligand has effect on residue MSF. Two-way ANOVA is also repeated for individual subunits, yielding p-value of 0.0456 for subunit A and 0.0000 for subunit B, again confirming the effect of bt10 on MSF.

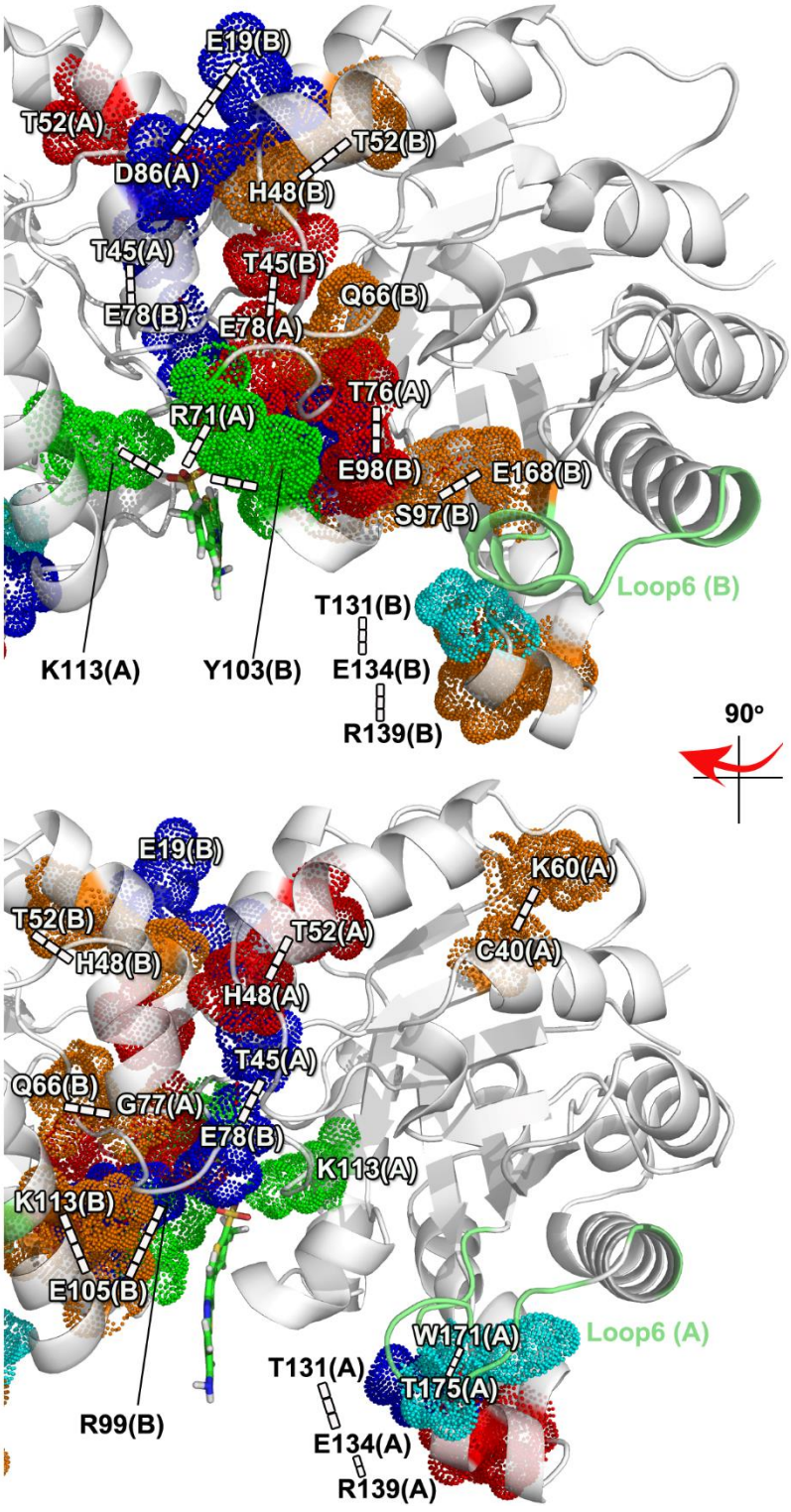

Figure S3. Details of the changes in H-bonding network are shown for subunit A (bottom) and B (top). Detailed version of Figure 1-e, where the residue pairs listed in Table S2 are labeled.

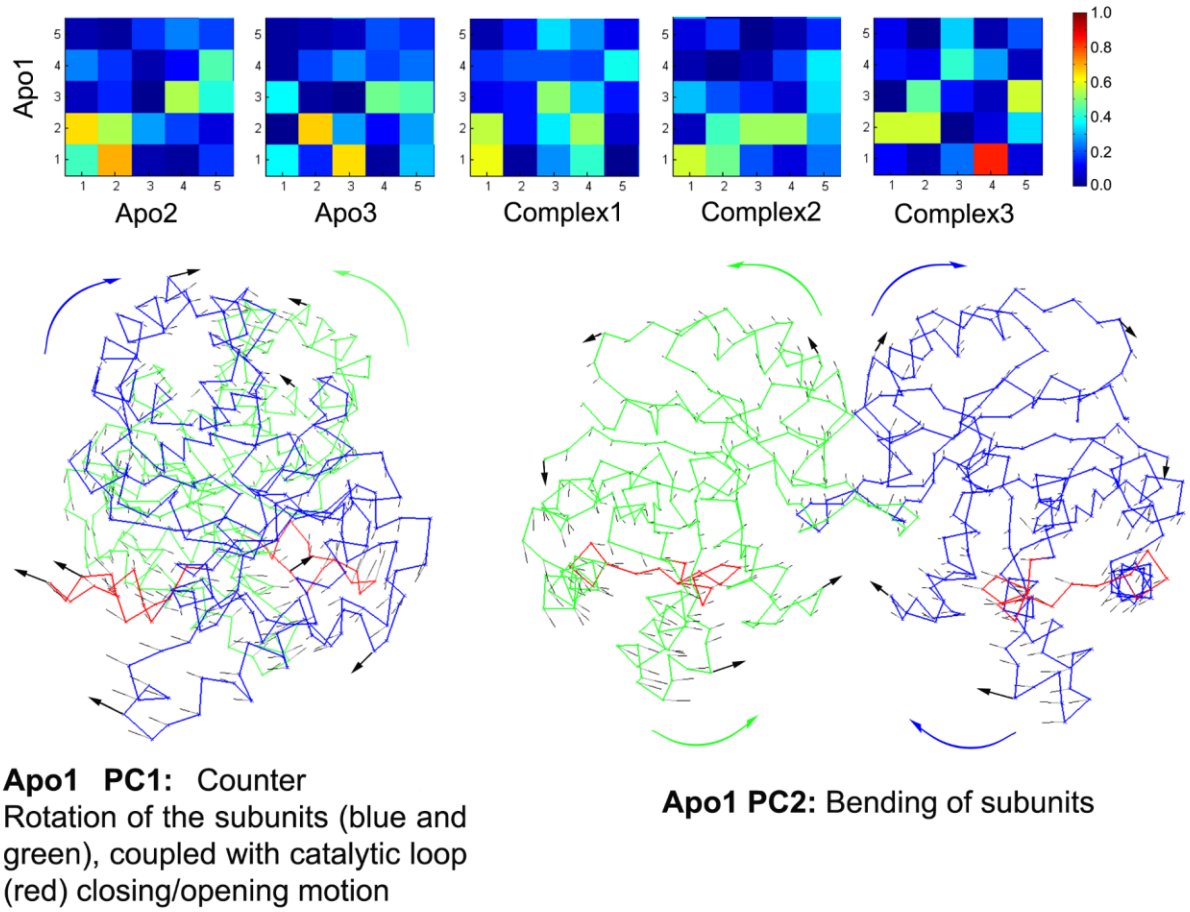

Figure S4. PCA mode overlap matrices with reference to Apo1 PCs. Counter rotation of the subunits, coupled with loop 6 opening/closure event over the active site, corresponds to the first PC in Apo1, second in Apo2 and third in Apo3 (side view). This mode is also present in complex simulations, but either with overlap value less than 0.6 (Complex1 and Complex2) or with high overlap but less contribution (Complex3). Contribution of each PC to overall motion is given in Table S3. Another dominant motion is the bending of the subunits (second PC in Apo1), where the lateral movement of the loop 6 is observed (front view). It should be noted that longer runs are necessary for the convergence of essential modes determined by PCA.

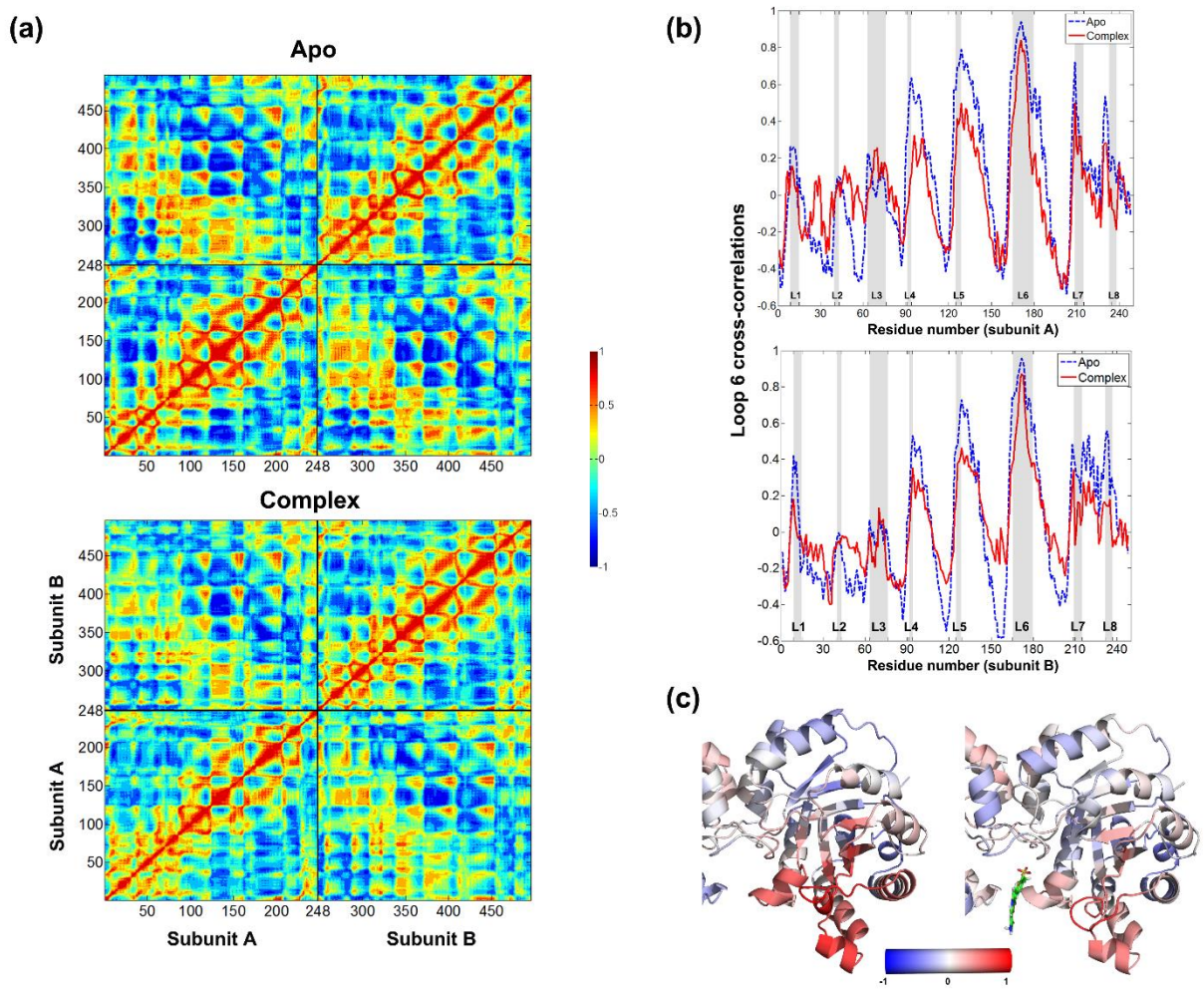

Figure S5. Residue-residue orientational cross-correlations based on the cumulative action of first five PCs, reported as averages over three independent runs. (a) Intra- and inter-subunit cross-correlations are shown for apo and complex runs. Presence of inhibitor at the interface often decreases the strength of correlations. (b) Orientational correlations of loop 6 tip residues with other regions, given separately for subunits A and B. This plot represents an average over residues Ile173-Gly174-Thr175, which is based on first five PCs in (a) panels. The ligand decreases the coordination of loop 6 within itself and with other regions including loops 7 and 8. (c) Correlations of loop 6 tip residues color-coded on subunit A for apo and complex simulations (subunit B given in Figure 3-d).

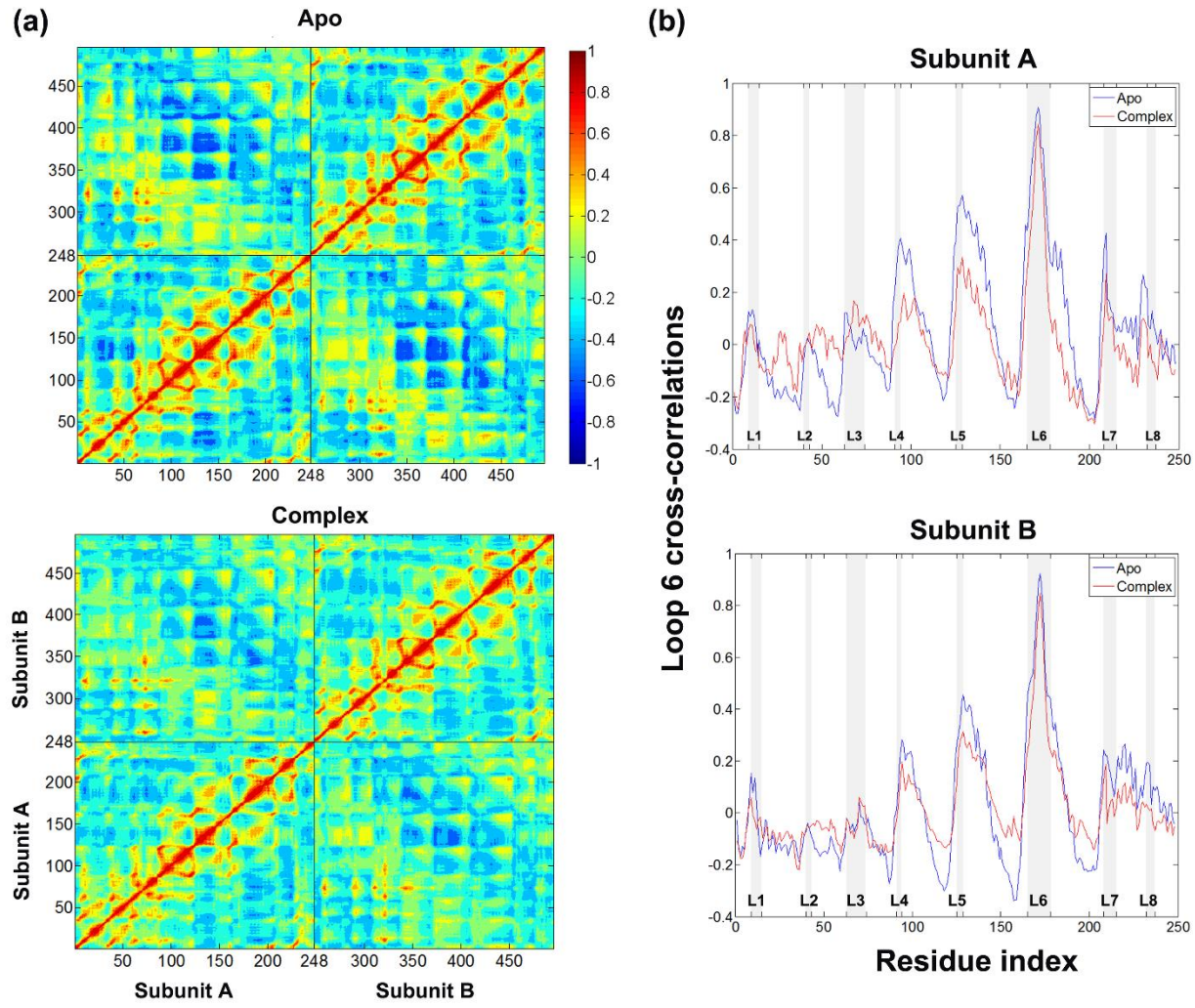

Figure S6. Residue-residue orientational cross-correlations based on the cumulative action of the PCs that contribute to 90% of total motion (more than 100 PCs, see Table S3), reported as an average over three independent runs (apo and with ligand). The figure shows a similar trend as in Figure S5 (plotted using the first 5 PCs), for both inter and intra cross-correlations of both subunits and loop 6.

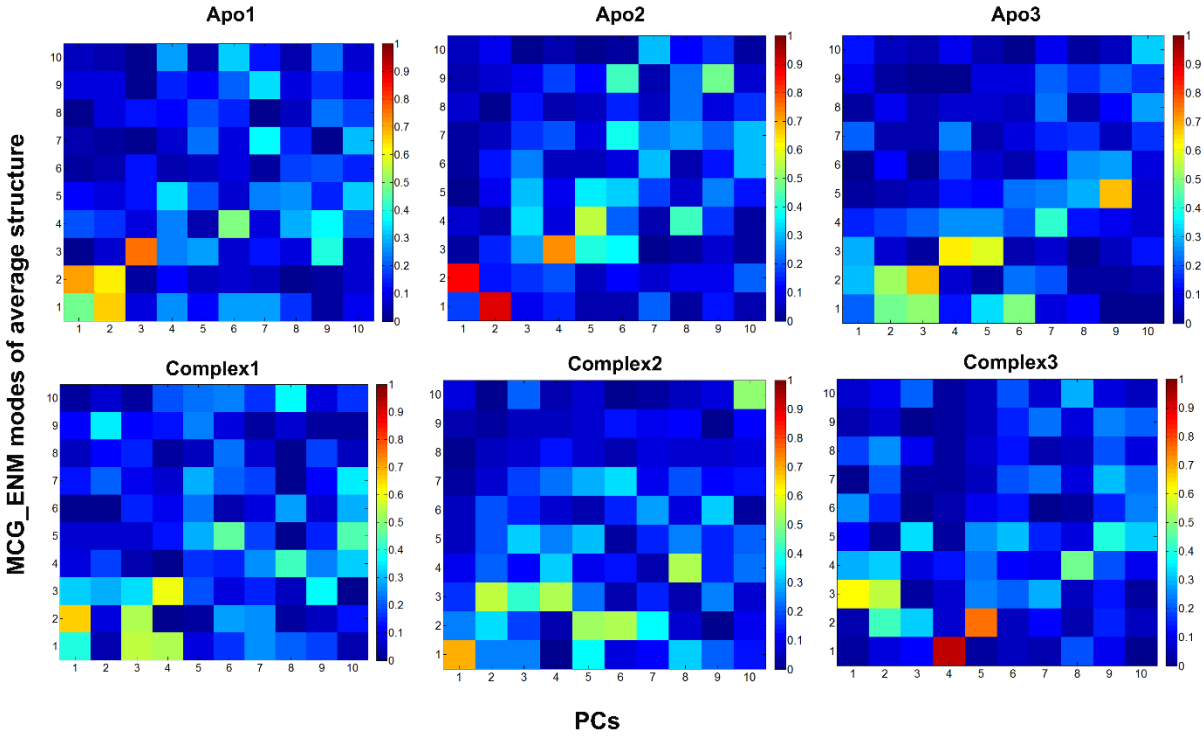

Figure S7. Overlap matrices between MCG_ENM modes and PCs plotted for each run. MCG_ENM modes are based on the average structure of each run. Especially the first three ENM modes exhibit an overlap value greater than 0.5 at least with one of the first 5 PCs on the 100 ns timescale. The MCG_ENM takes into account the average structure of the ligand in the complex runs.

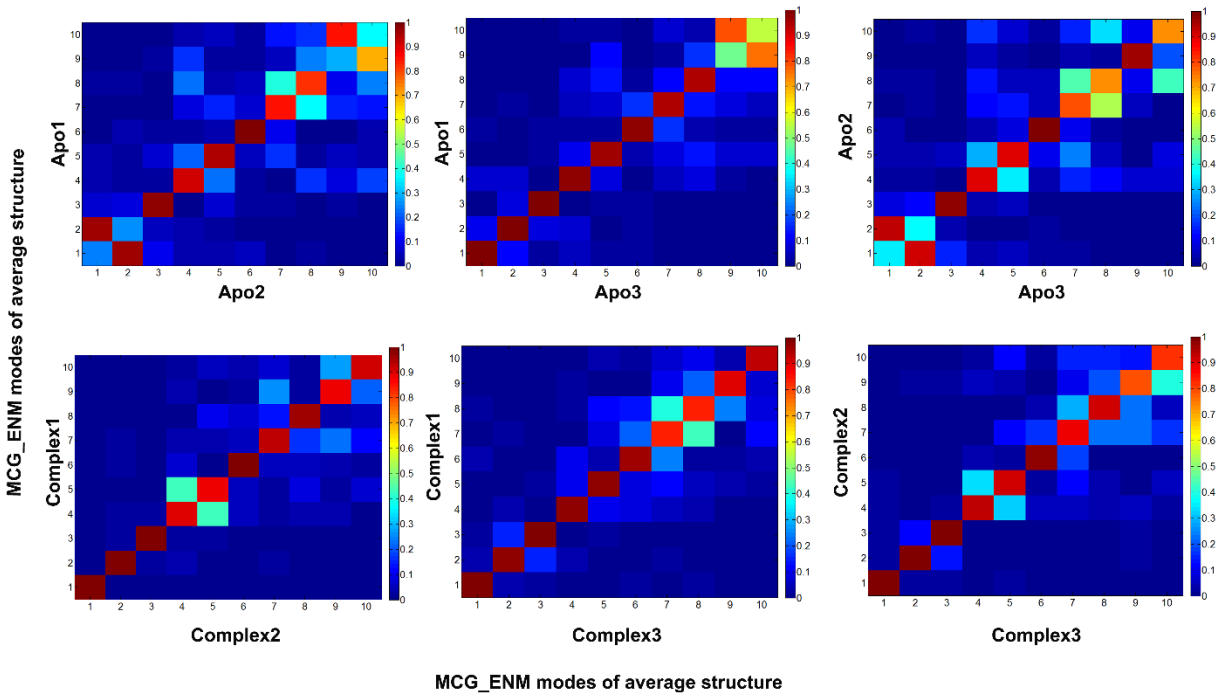

Figure S8. Overlap matrices among MCG_ENM modes of different MD runs (based on each run's average structure). Although there is not a one-to-one correspondance between the PCs of apo and complex runs (Figure S4), MCG_ENM modes are fully conserved among apo runs (top panels), as well as complex ones (bottom panels). Therefore, we used MCG_ENM instead of PCA to observe the changes in global modes due to ligand binding, as shown in the next figure.

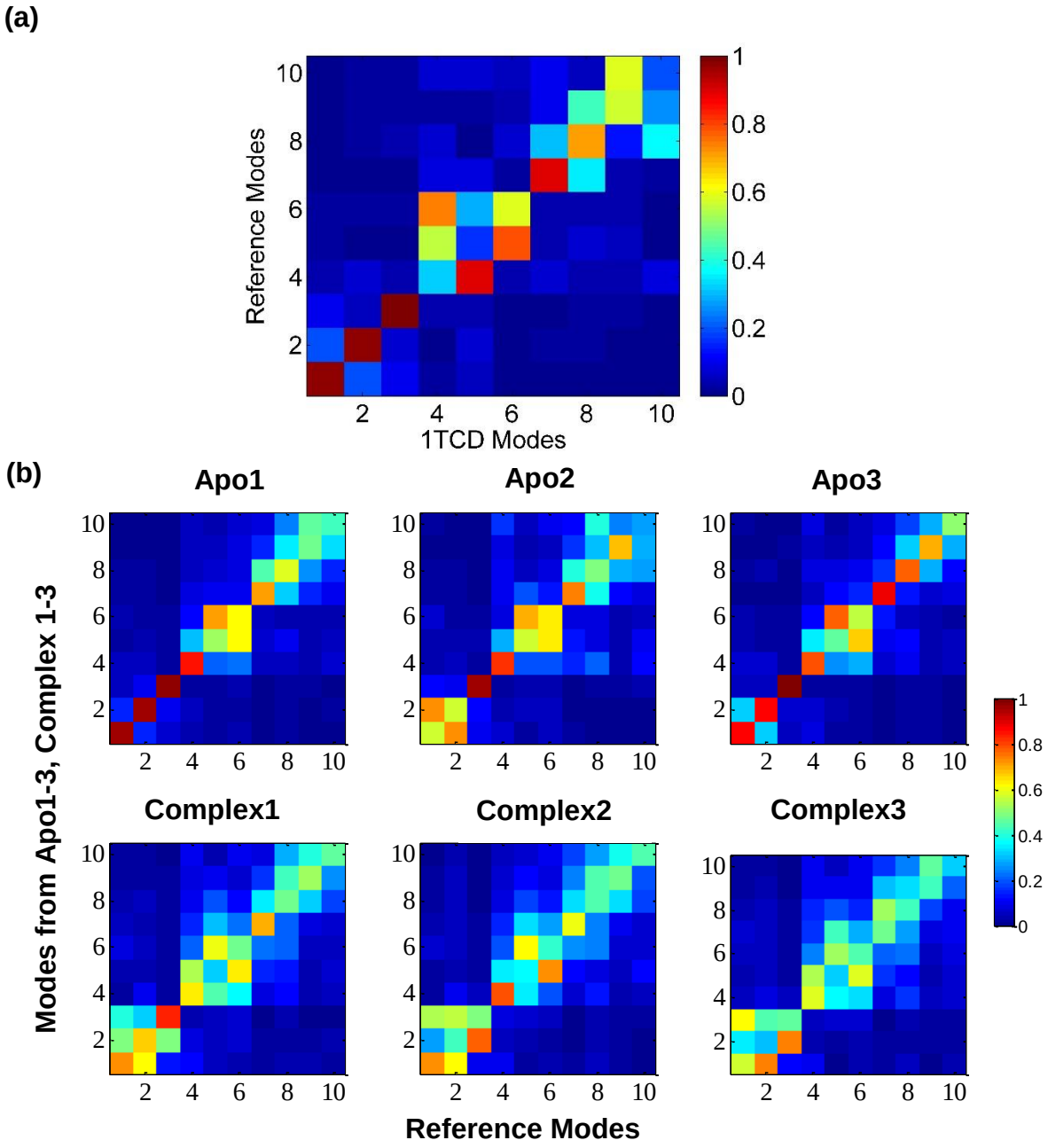

Figure S9. Overlap matrices for reference modes (RMs from Apo1 10th ns structure) from MCG_ENM. (a) Overlap matrix between RMs and ENM modes of crystal structure (1tcd). RMs are matching to 1tcd modes, indicating that 10th ns structure of Apo1 is an appropriate choice for reference. (b) Mean overlap matrices between MCG_ENM modes of each snapshot and the reference modes. Average overlap value for each entity is obtained as an average over 9000 frames of a specific run. Figure 2-b in the text presents further averaging over three apo or complex runs (upper/ lower matrices). The RMs are more conservative in apo runs. Issues on mode swapping and change in mode character are given in Table S4.

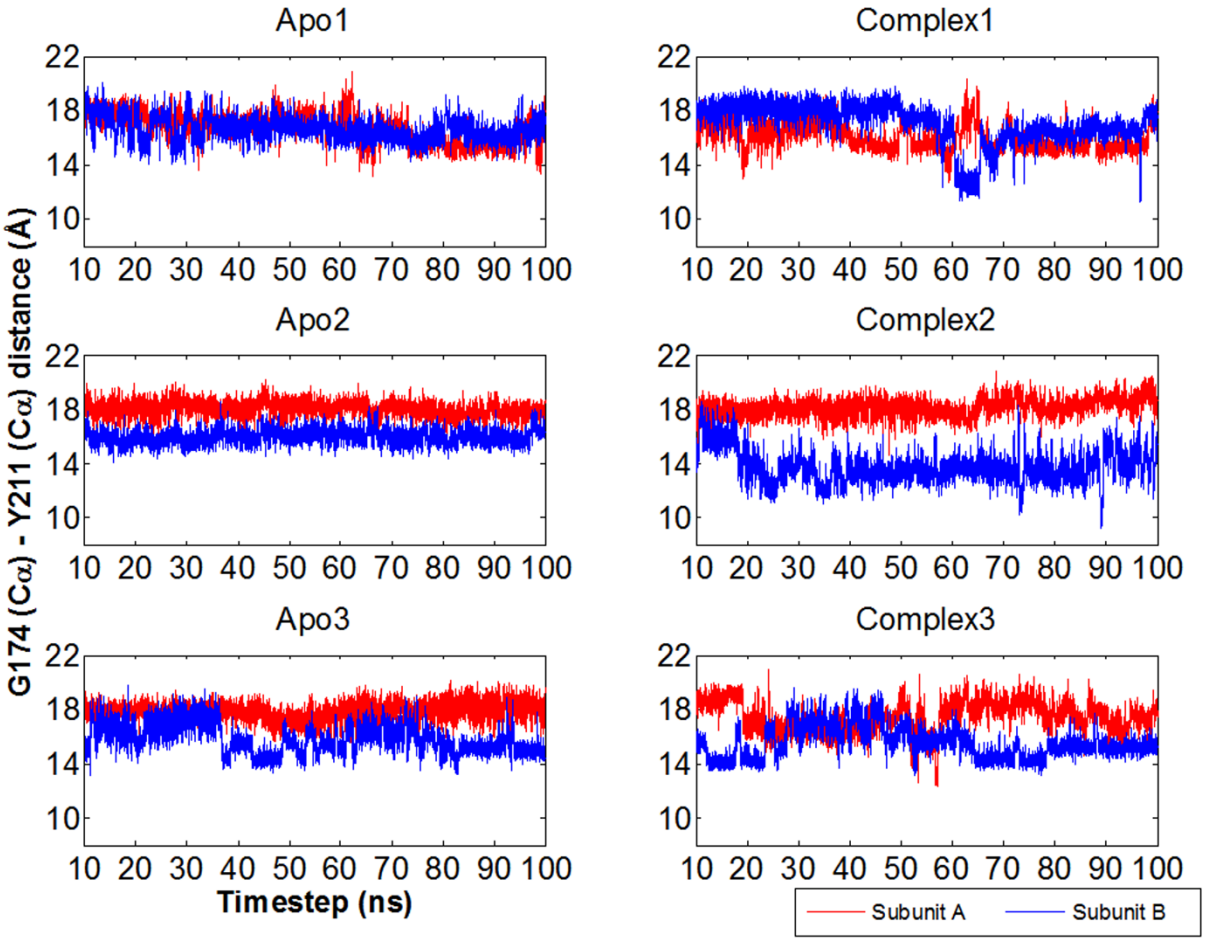

Figure S10. Loop 6 opening and closure is observed in the monomers based on the distance between loop's tip residue G174 and a relatively immobile residue Y211. The loop samples lower distances in the complex runs.

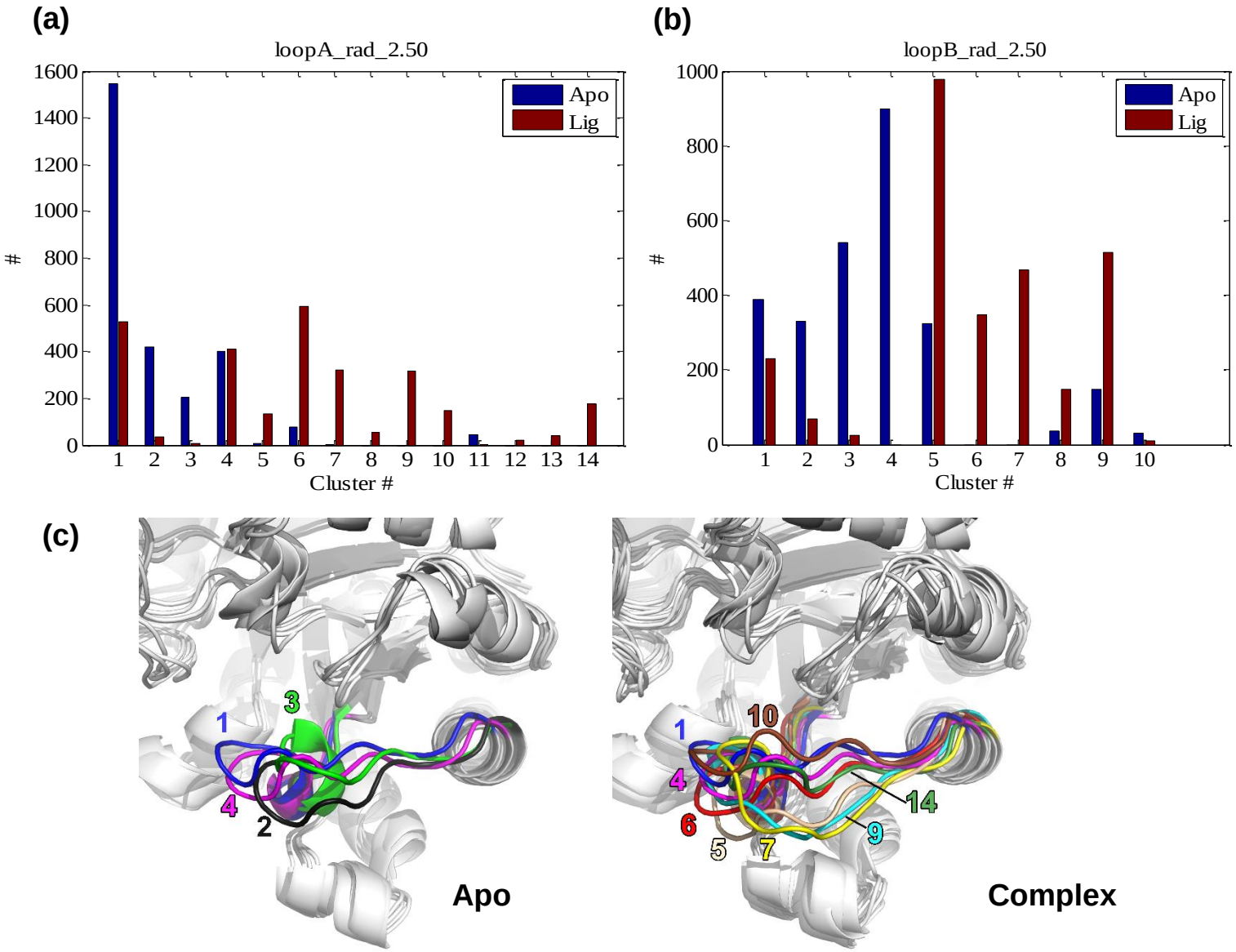

Figure S11. Clustering of loop 6 conformers for (a) subunit A and (b) subunit B for apo and complex (over 5400 snapshots in total). Clustering is performed based on mutual RMSD with 2.5 Å cutoff, after alignment of each monomer. (c) Loop 6 clusters sampled in apo and complex simulations for subunit A (see Figure 3-c for subunit B). In both subunits, complex and apo conformers belong to distinct clusters, hinting a causality between inhibitor presence and loop 6 conformational change.

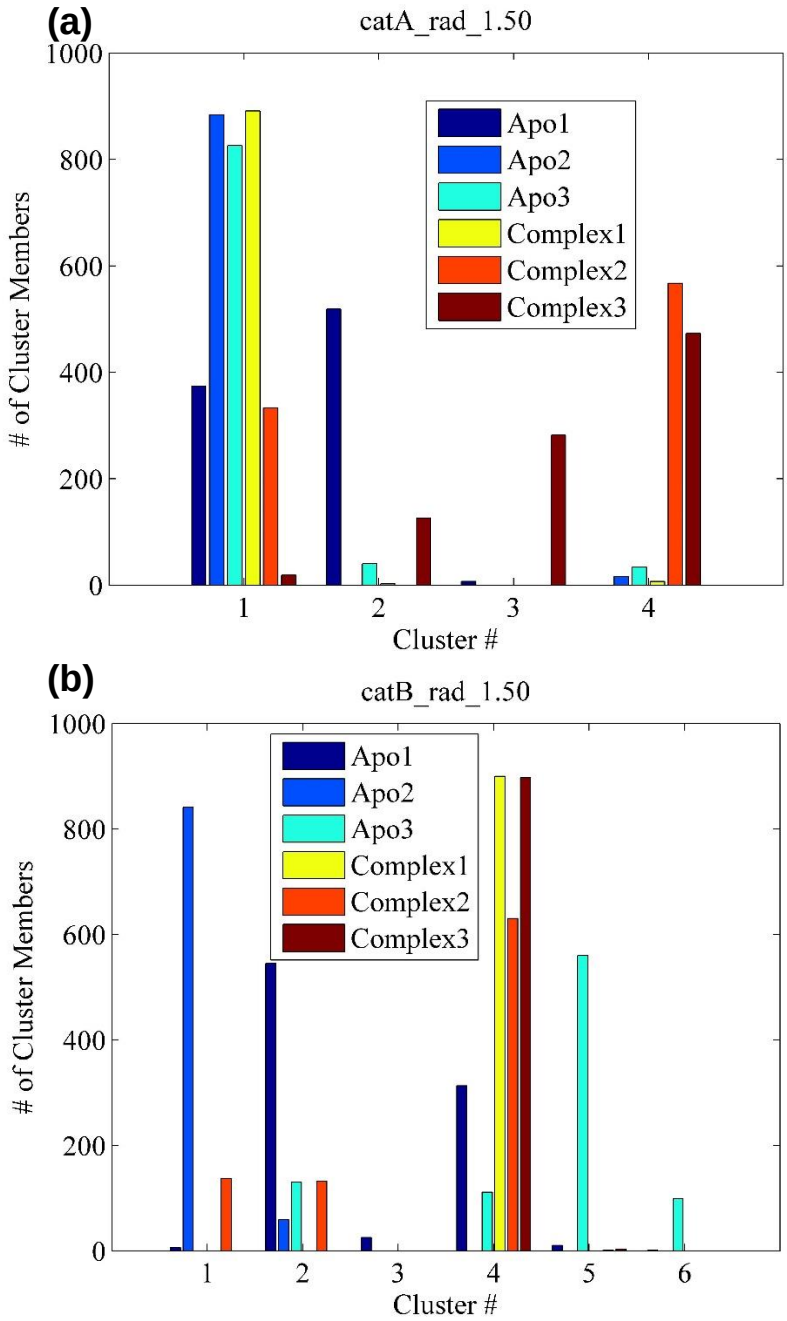

Figure S12. Clustering of catalytic residues Asn12, Lys14, His96 and Glu168 for (a) subunit A and (b) subunit B for apo and complex runs (over 5400 snapshots in total). Clustering is performed based on mutual RMSD with 1.5 Å cutoff, after alignment of each monomer. Clusters (presented in Figure 4-b), indicating that apo and complex simulations sample distinct conformers. For subunit B, the complex runs mostly fall in cluster #4, hinting to a constraining effect on the catalytic residues.

TABLES

Table S1. System details for MD simulations

MD runs	Total number of atoms	Number of water molecules	Final box dimensions (Å)	Initial structure[a]
Apo1	54980	15753	89	1tcd
Apo2	54830	15711	89	2 ns of Apo1
Apo3	57554	16611	90	11 ns of Apo1
Complex1	59274	17170	91	D1 (1)
Complex2	61282	17842	92	D3 (1)
Complex3	59848	17364	91	0.5 ns of Complex2

[a]Apo1 simulation started from the x-ray structure with pdb id 1tcd at 1.83 Å resolution. Initial structures for Apo2 and Apo3 simulations were taken as Apo1 snapshots at 2 and 11 ns, respectively. For TcTIM-bt10 complex simulations, we used bt10-docked structures from our previous docking study (1), which were named as "D1" (7 ns of Apo1, bt10 docked) and "D3" (13.5 ns of Apo1, bt10 docked) in that study and used as initial structures for Complex1 and Complex2, respectively. For Complex3, we used the snapshot at 0.5 ns of Complex2 as initial structure.

Table S2. Occurrence percentage of H-bonding residue pairs[a] that differ by more than 15% between apo and complex runs

Donor Residue	Acceptor Residue	Apo	Complex	Color
Glu19 (B) Main	**Asp86 (A) Side**	**37**	**13**	**Blue**
Cys40 (A) Main	Lys60 (A) Main	7	24	Orange
Thr45 (B) Side	**Glu78 (A) Main**	**12**	**44**	**Red**
Thr45 (A) Side	**Glu78 (B) Main**	**35**	**12**	**Blue**
Thr52 (B) Side	His48 (B) Main	35	51	Orange
Thr52 (A) Side	His48 (A) Main	31	53	Red
Thr76 (A) Side	**Glu98 (B) Side**	**55**	**81**	**Red**
Gly77 (A) Main	**Gln66 (B) Side**	**28**	**46**	**Orange**
Ser97 (B) Side	Glu168 (B) Side	38	57	Orange
Arg99 (B) Side	Glu105 (B) Side	43	6	Blue
Lys113 (B) Side	Glu105 (B) Side	26	42	Orange
Thr131 (A) Side	Glu134 (A) Side	49	14	Blue
Thr131 (B) Side	Glu134 (B) Side	36	16	Cyan
Arg139 (A) Side	Glu134 (A) Side	17	44	Red
Arg139 (B) Side	Glu134 (B) Side	24	39	Orange
Thr175 (A) Side	Trp171 (A) Main	35	17	Cyan

[a]H-bonding pairs are extracted using VMD Hydrogen Bonds analysis, where the default criterion of 3 Å distance between donor and acceptor and 20^{o} supplementary angle is used. Inter-subunit H-bonds are highlighted in bold.

Table S3. Individual and cumulative contributions of PCs to total motion

MD runs	PC1	PC2	PC3	PC4	PC5	Cumulative contribution of first 5 PCs	# of PCs that explain 90% of motion
Apo1	36.5	9.5	7.5	3.6	3.0	60	100
Apo2	17.0	15.6	6.6	5.0	4.0	48	139
Apo3	19.9	13.7	9.1	5.3	4.2	52	122
Complex1	21.2	14.5	6.0	3.9	3.0	49	134
Complex2	17.6	9.0	7.1	5.4	3.9	43	153
Complex3	27.2	10.5	6.6	5.1	4.0	53	109

Table S4. Conservation of RMs in MD snapshots using MCG_ENM

RM Index[a]	**% of mode shape conservation**[b]		**% of mode index conservation**[c]	
	Apo	Complex	Apo	Complex
1	98	74	70	47
2	99	71	70	21
3	100	99	100	50
4	94	73	85	54
5	87	69	11	0
6	64	53	16	3
7	91	67	78	46
8	58	33	45	17
9	67	41	52	24
10	13	11	11	10

[a] RMs are the reference ENM modes obtained from the 10th ns snapshot Apo1 run.

[b] The percentage of MD snapshots that present at least one ENM mode (among its first 10 modes) that highly correlates (overlap > 0.7) with a specific RM is reported for apo and complex runs. Through this calculation, changes in mode shapes can be detected because mode swapping is not considered. First four modes are almost always present in apo simulations. However, with bound-bt10, RM1, RM2 and RM4 change character in 25-30 % of the snapshots but RM3 is preserved.

[c] The percentage of MD snapshots that preserve both the mode shape (overlap > 0.7) and the mode index are reported with reference to each RM. The extent of mode swapping can be inferred from these numbers.

References

1. Kurkcuoglu, Z., G. Ural, D. Akten, and P. Doruker. 2011. Blind Dockings of Benzothiazoles to Multiple Receptor Conformations of Triosephosphate Isomerase from *Trypanosoma cruzi* and human. Mol. Inf. 30:986 – 995.